

---

# SHI-NESS: DETECTING GOOD AND STABLE KEYPOINTS WITH A NEURAL STABILITY SCORE

---

A PREPRINT

**Konstantin Pakulev**  
Center for AI Technology (CAIT)  
Skolkovo Institute of Science and Technology  
Moscow, Russia 121205  
Konstantin.Pakulev@skoltech.ru

**Alexander Vakhitov**  
SLAMcore  
London, United Kingdom SE1 1JA  
alexander.vakhitov@gmail.com

**Gonzalo Ferrer**  
Center for AI Technology (CAIT)  
Skolkovo Institute of Science and Technology  
Moscow, Russia 121205  
G.Ferrer@skoltech.ru

April 19, 2021

## ABSTRACT

Learning a feature point detector presents a challenge both due to the ambiguity of the definition of a keypoint and correspondingly the need for a specially prepared ground truth labels for such points. In our work, we address both of these issues by utilizing a combination of a hand-crafted Shi detector and a neural network. We build on the principled and localized keypoints provided by the Shi detector and perform their selection using the keypoint stability score regressed by the neural network - Neural Stability Score (NeSS). Therefore, our method is named Shi-NeSS since it combines the Shi detector and the properties of the keypoint stability score, and it only requires for training sets of images without dataset pre-labeling or the need for reconstructed correspondence labels. We evaluate Shi-NeSS on HPatches, ScanNet, MegaDepth and IMC-PT, demonstrating state-of-the-art performance and good generalization on downstream tasks. We will share our code upon acceptance of the paper.

**Keywords** Keypoint detection · Sparse local features · Self-supervised learning

## 1 Introduction

Feature point detection (keypoint detection) is usually the first step in camera localization and scene reconstruction pipelines based on sparse features, commonly used in robotics [1], computer vision [2], augmented, mixed and virtual reality [3, 4], and other systems.

Whilst feature description is successfully approached in the literature as a metric learning [5, 6] problem, applying deep learning to the feature detection task still poses a challenge, with classical solutions showing competitive results on the state-of-the-art benchmarks [7]. The difficulty is caused by the innate vagueness of the point of interest definition [8] which greatly complicates the formulation of feature detection as a learning problem.

The data required to learn keypoints with sufficient robustness to illumination and viewpoint changes presents another challenge. Structure-from-Motion (SfM) [2, 9] and Multi-View Stereo (MVS) [10, 9] reconstructions that are used by some methods [11, 12, 13, 14, 15] to obtain pixel-accurate correspondences are hard to build properly and lack full image coverage [16, 17].

We approach the problem of “defining a keypoint” by leveraging principled assumptions that make up reasonable keypoints [18]: we employ the Shi [18] detector to provide locations for keypoints as well as to perform sub-pixel localization. At the same time, we propose a quantitative metric to measure the stability of the detected keypoints, the *keypoint stability score*, that randomly perturbs the detected points and its surrounding patches for later aggregation of their statistics. This metric, can be calculated in an online fashion and from a single image, so it is ideal for automatically generating a supervised signal to train a neural network that predicts it, the Neural Stability Score (NeSS).

Shi-NeSS empowers a classical method with a neural approach, that together obtain accurate locations of keypoints that are more likely to remain stable under viewpoint changes. Compared to the prior art, Shi-NeSS needs only a set of real images for training, without any labels, ground-truth poses or reconstructed correspondences.

In our work, we present the design that does not rely on ground truth point correspondences alongside [19, 20, 21]. These methods are sometimes referred to as self-supervised [19, 21]. Out of self-supervised methods only Key.Net [20] and REKD [21] work in a similar setting, while SuperPoint [19] relies on pre-labeled datasets and requires pre-training a base detector on a synthetic dataset (see Table 1).

Our contributions are as follows. We present a novel metric, the Keypoint Stability Score, to estimate the quality of keypoints. We propose a method to directly learn keypoint stability scores in a neural network, which requires only images for training. In terms of pose accuracy, it surpasses state-of-the-art on MegaDepth [16], is on par on IMC-PT [7], ScanNet [17] and HPatches [22], being the best among the self-supervised methods.

Methods	Pre-training base detector	Dataset pre-labeling	Ground-truth generation
SuperPoint [19]	Yes	Yes	Offline
Key.Net [20]	No	No	Offline
REKD [21]	No	No	Offline
Shi-NeSS	No	No	Online

Table 1: Comparison of self-supervised methods for learning keypoints.

## 2 Related works

### Handcrafted detectors.

Since Moravec [23], feature detection methods focused on finding the local extrema in the signals derived from images that correspond to meaningful structures, e.g. corners [8]. Therefore, the earliest designs of detectors employ the grayvalue analysis via differential expressions [8, 24, 25, 18, 26].

Among those, Harris [24] and Shi [18] detectors state that good features should be ‘trackable’, i.e. strongly distinguishable in a small image neighbourhood, and the methods [27, 28, 29] follow this idea. We employ the Shi detector for finding keypoint candidate locations due to its efficiency.

Depending on the image resolution or scale both the location and the strength of keypoints response change [8]. The most productive way to tackle this problem is the modeling of scale via the Gaussian scale-space [26] - the backbone of some famous methods like SIFT [30], SURF [31], Harris-Laplace [28], Harris-Affine [29], KAZE [32]. In our method, instead of using the scale space maxima, we predict a score using the neural network that assesses the stability of a point to viewpoint changes (see Sec. 3.2).

**Learned detectors.** Existing designs of learned detectors are quite diverse. The majority of the methods employ correspondence labels for training which are obtained via SfM and MVS [11, 12, 14, 15], or optical flow [13]. Preparing dense pixel-accurate ground-truth correspondence labels poses the problem by itself [10, 9] - special pre-processing of the data and validation of the obtained results is required [13, 17, 16]. Although avoiding the surface reconstruction can ease the problem formulation [2, 10] accurate poses can still be hard to obtain [33]. In this regard, methods that do not require reconstructed correspondences, such as [19, 20, 21], or the method proposed here, present a viable alternative.

SuperPoint [19] relies on Homographic Adaptation, i.e. generation of homographies for creating correspondences, to train on real images with supervision from a base detector trained on synthetic data. Key.Net [20] creates a dataset of image patches by generating homographies and employs hand-crafted filters for finding potential keypoints, using scale space modeling. Our approach doesn’t require pre-labeling or creating synthetic datasets or designing a base detector, and it does not use any scale-space analysis. We modify the Homographic Adaptation and generate the required correspondences online during the training, leveraging a specially designed keypoint quality measure. REKD [21]

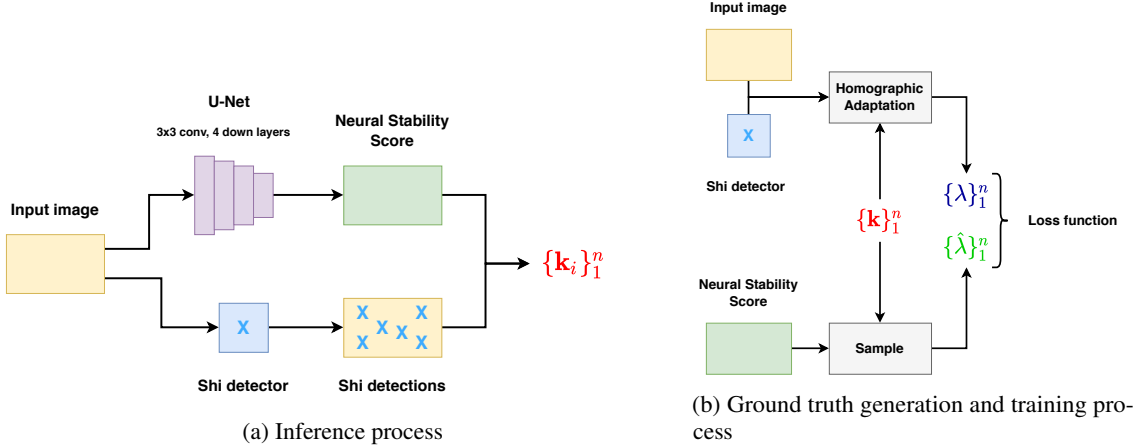


Figure 1: 1a The method takes an image, applies Shi detector to get locations of keypoints and to perform sub-pixel localization. Simultaneously, it uses the neural network to regress the Neural Stability Score. A set of the best feature points  $\{\mathbf{k}_i\}_1^n$  is selected from detected points according to the learned score. 1b For the selected points we obtain stability scores  $\{\lambda_i\}_1^n$  using the modified Homographic Adaptation and the Shi detector. At the same time, we sample the Neural Stability Score at locations  $\{\mathbf{k}_i\}_1^n$  obtaining learned estimates  $\{\hat{\lambda}_i\}_1^n$ . Finally, the loss function is applied to  $\{\lambda_i\}_1^n$  and  $\{\hat{\lambda}_i\}_1^n$ .

uses a rotation-equivariant network to detect keypoints together with orientations, using image sets without additional annotations for training similarly to our method.

### 3 Method

Shi-NeSS is a combination of the hand-crafted Shi detector and a neural network (see Fig. 1). We briefly present the formulation of the Shi detector as well as describe the sub-pixel localization procedure in Sec. 3.1. In Sec. 3.2 we describe the measure that allow to quantitatively assess keypoints, the keypoint stability score. Sec. 3.3 discusses the training process of the neural network which aims to predict the keypoint stability score, the neural stability score (NeSS), and Sec. 3.3 describes the training process. Finally, Sec. 3.4 gives an account of implementation details.

#### 3.1 Shi detector

We use the Shi detector to get the locations of feature points. For each pixel we calculate the second-moment matrix using the Gaussian weighting function [24, 18] and assign it with a score that is equal to the smallest eigenvalue of the second-moment matrix [18]. By applying the non-maximum suppression over the obtained score map we get the required locations of keypoints.

We further refine locations of feature points following [30]. By performing the second order Taylor expansion of the Shi score function  $\mathcal{S}(\mathbf{x})$  around a point  $\mathbf{x}$  we can find the correction  $d\mathbf{x}$  that maximizes  $\mathcal{S}(\mathbf{x})$  by solving:

$$d\mathbf{x} = -\frac{\partial^2 \mathcal{S}^{-1}}{\partial \mathbf{x}^2} \frac{\partial \mathcal{S}}{\partial \mathbf{x}}. \quad (1)$$

To avoid unnecessary calculations the sub-pixel localization procedure is applied only to the best-k feature points selected according to the keypoint stability score regressed by the neural network (Neural Stability Score). We describe the scores in the next sections.

#### 3.2 Keypoint Stability Score

In this work, we design a quantitative description to assess feature points detected by the Shi detector. Given a keypoint  $\mathbf{k}$  we apply to it a set of generated homographies  $\{\mathcal{H}_j\}_1^m$  to produce a set of  $m$  warped keypoints  $\{\mathbf{k}'_j\}_1^m$ :

$$\mathbf{k}'_j = \mathcal{H}_j \mathbf{k}. \quad (2)$$

We generate homographies using a modified Homographic Adaptation procedure of SuperPoint [19] by sampling random perspective distortions while restricting the deformation along x- and y- axes. We do not add rotation or translation transformations since the Shi detector with Gaussian weighting is invariant to them [24, 18, 27].

Next, we create a grid  $\mathbf{G}_j$  of the predetermined size  $s_{patch}$  around each of the warped points  $\mathbf{k}'_j$ , warp the grid back to the image coordinates and sample values in these locations to get a deformed patch  $\mathbf{P}_j$  around  $\mathbf{k}'_j$ :

$$\mathbf{P}_j = \text{sample}(\mathcal{H}_j^{-1} \mathbf{G}_j). \quad (3)$$

The Shi detector is not invariant to scale [27] or perspective transformations. Hence, in general, we cannot compare its responses from different patches and have to consider only locations of maximum responses. We run the Shi detector  $f_{Shi}$  on each patch getting a score map  $\mathbf{S}_j = \{\mathbf{s}_i\}_1^{s_{patch}}$  and extract from it the location  $\hat{\mathbf{l}}_j$  that corresponds to the maximum activation:

$$\hat{\mathbf{l}}_j = \underset{\mathbf{s}_i}{\text{argmax}} f_{Shi}(\mathbf{P}_j). \quad (4)$$

Next, we warp each  $\hat{\mathbf{l}}_j$  back to the original reference frame and calculate the sample covariance  $\Sigma$  with respect to the original position  $\mathbf{k}$ :

$$\Sigma = \sum_{j=1}^m \frac{(\mathcal{H}_i^{-1} \hat{\mathbf{l}}_j - \mathbf{k})(\mathcal{H}_j^{-1} \hat{\mathbf{l}}_j - \mathbf{k})^\top}{m-1}. \quad (5)$$

Finally, we can characterize a feature point by the largest of eigenvalues  $\lambda_1$  and  $\lambda_2$  of  $\Sigma$ :

$$\lambda = \max(\lambda_1, \lambda_2) = \|\Sigma\|_2. \quad (6)$$

The keypoint stability score  $\lambda$  captures the maximum variation of a point from its location under perspective transformations of its neighbourhood. The measure prioritizes feature points that deviate the least from the initial location  $\mathbf{k}$  in any direction and, hence, are more likely to be accurately detected and localized.

Since  $\lambda$  assesses keypoints based on their local perturbations, the patch of size  $s_{patch}$  is set to be small. This particular trait makes a foundation for the training process of the Neural Stability Score regression network, which is discussed next.

### 3.3 Training process: Neural Stability Score

Providing full ground-truth labeling with  $\lambda$  of every pixel of every full-resolution image in a dataset using our method can be computationally expensive. So instead, in line with several works [12, 15], we select a number of feature points during the training using the trained-so-far weights of the model. More specifically, for each image we extract  $n$  feature points  $\{\mathbf{k}_i\}_1^n$ , Shi scores  $\{\mathbf{s}_i\}_1^n$  and the Neural Stability Scores provided by the neural network  $\{\hat{\lambda}_i\}_1^n$  (see Fig. 1). Relying on the Shi detector allows to faster guide the neural network towards better points in the beginning of the training.

For each point  $\mathbf{k}_i$  we calculate the ground-truth stability score  $\lambda_i$  using the keypoint Stability Score (Eq. 6). Due to the small size of  $s_{patch}$  we can use a large number of samples for the calculation of  $\Sigma_i$  as well as apply the same set of generated transformations  $\{\mathcal{H}_j\}_1^m$  to all extracted feature points  $\{\mathbf{k}_i\}_1^n$  simultaneously. The combination of online feature extraction and fast calculation of  $\lambda$  allows us to avoid time-consuming dataset pre-labeling.

Not every point with a good  $\lambda$  score makes a good training target - image artifacts due to the absence of photometric changes in the generation procedure of the keypoint stability score can be stable as well. A common trait of these points is that they tend to have low salience and, hence, can be filtered out by the Shi detector assuming a threshold  $t_{Shi}$ . We define  $\mathbb{1}(s_i > t_{Shi})$  as an indicator function that gives 1 if  $s_i$  larger than  $t_{Shi}$  and 0 otherwise. Applying filtering considerably improves the performance of the method, see details in the supplementary material.

Finally, we learn  $\{\hat{\lambda}_i\}_1^n$  by formulating the training objective as a regression problem:

$$L = 0.5 \frac{\sum_{i=1}^n (\hat{\lambda}_i - \lambda_i)^2 \mathbf{1}(s_i > t_{Shi})}{\sum_{i=1}^n \mathbf{1}(s_i > t_{Shi})}. \quad (7)$$

### 3.4 Implementation details

We train our detector from scratch on the same subset of MegaDepth dataset [16] as used in DISK [15]. We do not use poses, depth maps or any other information from the dataset other than images. For training we use full-resolution images cropped to a square of length 560 pixels. We perform validation and model selection on the validation subset of the IMC-PT dataset [7].

In the implementation we set  $s_{patch}$  equal to the size of the non-maximum suppression kernel - 5. However, since we need to calculate the Shi responses for each pixel of  $\mathbf{P}_j$  the actual patch size needs to be larger - for our configuration of the Shi detector that value is 11. Hence, we warp the larger grid to get  $\mathbf{P}_j$  but when doing the maximum extraction (see Eq. 4) we consider only the square with size  $s_{patch}$  pixels around its center. We choose  $n = 1024$  and  $m = 100$ , see the details in the supplementary material.

When extracting keypoints for convenience of the implementation instead of using  $\hat{\lambda}$  directly we consider  $e^{-\hat{\lambda}}$ .

We use a typical U-Net architecture [34] with 4 down-sampling layers and 3x3 convolutions. To train the model we employ Adam [35] optimizer with learning rate  $10^{-4}$ . The model that is used in evaluations in Sec. 4 was trained on a single NVIDIA 2080 Ti GPU for 22 hours (including validations).

In this section we have briefly introduced the Shi detector with sub-pixel refinement, defined the novel keypoint reliability metric - the keypoint stability score, described the Neural Stability Score as an approximation of the keypoint stability score with the help of the neural network, and outlined the implementation details of the neural network. We will proceed with the experimental evaluation of Shi-NeSS.

## 4 Experiments

The means of detector evaluation deserve special attention. Originally, detectors were mostly evaluated using classical metrics like repeatability and matching score [36]. Since feature points require supplying them with a description in order to obtain the correspondences a descriptor has to be accounted for to ensure the proper assessment of the quality of detected keypoints. A common solution is to fix a descriptor for all detectors in the evaluation [36, 37, 38, 20]. More recent publications reported evidence that gains in classical metrics do not necessarily translate to the gains in the downstream tasks performance [7]. For this reason, in our work, we mostly perform the evaluation on a range of downstream tasks. To get a more comprehensive assessment we test our method on a variety of datasets and tasks.

Image resolution plays an important role in the accuracy of correspondences, thus we provide images in the original resolution to all methods in our evaluation. It also allows to assess the ability of a detector to generalize beyond the training resolution. The number of keypoints that is extracted from each image plays no lesser role: we found the regime of 2048 keypoints per image from [7, 15] to be a good trade-off between the performance and the consumption of computational resources. To compute matches we use mutual nearest neighbour matching and employ the Lowe ratio test [30] for downstream tasks [7]. As choosing proper hyper-parameters for a method is of utmost importance for downstream tasks [7] we employ a hyper-parameter tuning procedure similar to one in [7].

In our evaluation we consider the following methods: Shi [24, 18], SIFT [30], SuperPoint [19], R2D2 [13], Key.Net [20], DISK [15] and REKD [21]. We extract feature points for all methods using only the original scale with the exception of Key.Net [20] and REKD [21] that have multi-scaling as an essential built-in part of the method. To ensure fair comparison we do not employ the orientation estimation for REKD [21] since other methods in the evaluation don't have it. As long as the sub-pixel localization is a part of our solution, the version of the Shi [24, 18] detector employed in our evaluation includes it since we focus on assessing the influence of the Neural Stability Score.

### 4.1 Evaluation on HPatches dataset

HPatches [22] dataset features sequences with planar surfaces related by homographies under a variety of illumination and viewpoint changes. We use the same test subset as in [14] totaling 540 image pairs among which 260 image pairs are with illumination changes and 280 - with viewpoint.

DISK [15] descriptor shows the state-of-the-art performance on HPatches thus we pick it for this dataset.

Methods	Overall mAA (5px)	Illumination mAA (5px)	Viewpoint mAA (5px)
Shi [24, 18] + DISK [15]	<b>0.716</b>	<b>0.892</b>	<b>0.552</b>
SIFT [30] + DISK [15]	0.688	0.877	0.512
SuperPoint [19] + DISK [15]	<b>0.706</b>	0.883	0.541
R2D2 [13] + DISK [15]	0.690	<b>0.888</b>	0.506
Key.Net [20] + DISK [15]	0.678	0.844	0.524
DISK [15]	0.699	0.867	<b>0.542</b>
REKD [21] + DISK [15]	0.689	<b>0.895</b>	0.498
Shi-NeSS + DISK [15]	<b>0.714</b>	0.883	<b>0.556</b>

Table 2: Homography evaluation on HPatches [22] with 2048 keypoints and full resolution images. We report mAA [42, 7] up to a 5 pixel threshold. Best results are marked in **red**, 2nd best - in **green**, 3rd best - in **blue**.

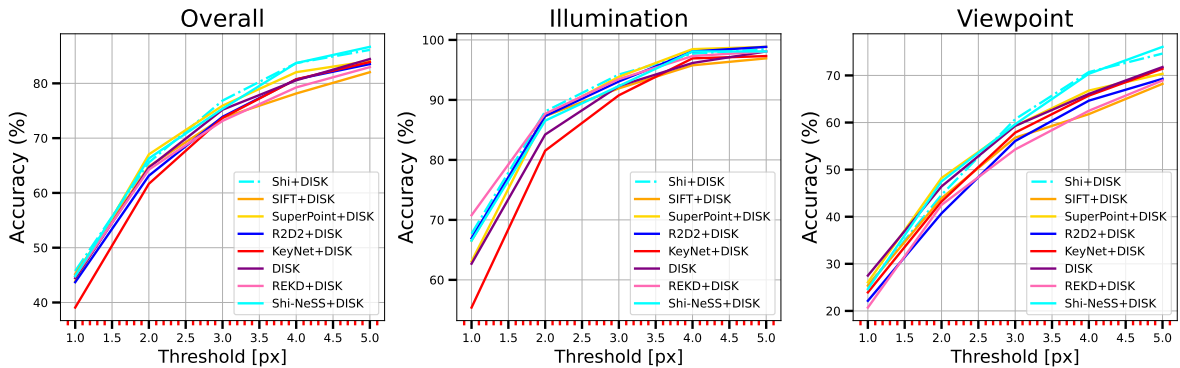


Figure 2: Evaluation on HPatches [22] with 2048 keypoints and full resolution images. We report homography estimation accuracy [19] in % for different categories.

We report Mean Matching Accuracy (MMA) [39, 14] under different pixel thresholds following [19, 14, 40, 15, 21]. Additionally, we evaluate on a downstream task of homography estimation using a protocol similar to [19, 40]. In particular, we get features, calculate a list of putative matches and use OpenCV’s [41] routines to estimate a homography. Next, we check the quality of the estimate by warping 4 image corners and calculating the average re-projection error compared to warping with the ground-truth homography [19]. We report accuracy as the percentage of image pairs out of the whole dataset with the average re-projection error lower than a threshold for different thresholds, thus, obtaining a curve. Additionally, we report mean Average Accuracy [42, 7] by integrating the curve up to a 5-pixel threshold to get a single-number quality measure for each category. For tuning hyper-parameters we use sequences of HPatches [22] left out from the test set [14] as well as hyper-parameters obtained from validation sequences of IMC-PT [7] on the task of relative pose estimation. This combination provides the best results for all methods, see details in the supplementary material.

**Results.** Compared to Shi [24, 18] detector that shows one of the best results on MMA our method considerably lags behind as illustrated in Fig. 3. However, evaluation on the task of homography estimation completely changes the ranking - our method shows strong performance on scenes with viewpoint changes (see Fig. 2 and Table 2). These results correlate with recent findings that classical methods can show state-of-the-art performance if tuned properly as well as that conventional metrics might not fully capture the complicated dependency between features and downstream tasks [7]. Still, it is worth noting that MMA evaluation highlights the lack of invariance of our feature points to illumination changes - this is reflected in the homography estimation evaluation as well. We believe that it is caused by the absence of illumination changes modeling in our method.

## 4.2 Relative pose evaluation

We evaluate on a downstream task of relative pose estimation following the protocol of [7]. We use our own evaluation pipeline to provide consistency in evaluations across different datasets. We take pairs of images, detect and describe

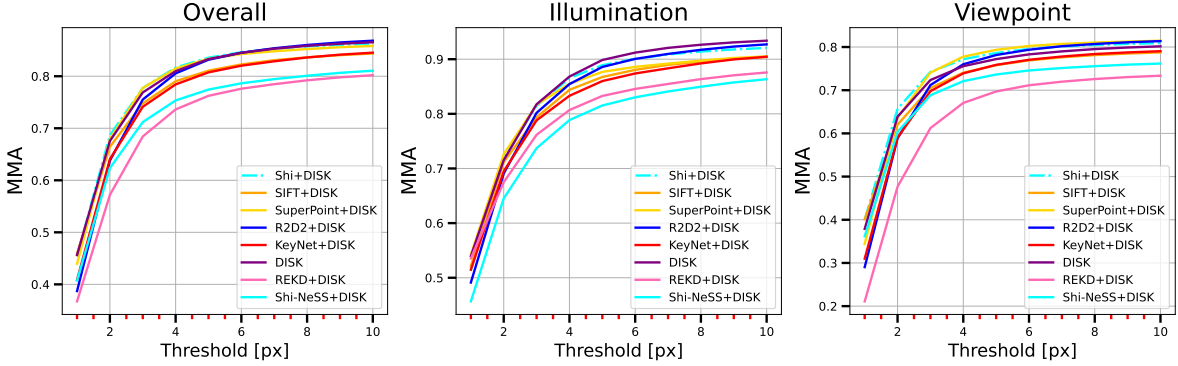


Figure 3: Evaluation on HPatches [22] with 2048 keypoints and full resolution images. We report MMA [39, 14] for different categories.

Methods	Rotation mAA (10°)	Translation mAA (10°)
Shi [24, 18] + DISK [15]	0.744	<b>0.422</b>
SIFT [30] + DISK [15]	0.7	0.387
SuperPoint [19] + DISK [15]	0.708	0.37
R2D2 [13] + DISK [15]	<b>0.751</b>	0.403
Key.Net [20] + DISK [15]	0.666	0.327
DISK [15]	<b>0.813</b>	<b>0.489</b>
REKD [21] + DISK [15]	0.601	0.271
Shi-NeSS + DISK [15]	<b>0.767</b>	<b>0.438</b>

Table 3: Evaluation on IMC-PT [22] with 2048 keypoints and full resolution images. We report mAA [42, 7] up to a 10 degrees threshold for rotation and translation. Best results are marked in **red**, 2nd best - in **green**, 3rd best - in **blue**.

features, calculate a list of putative matches, perform relative pose estimation and, finally, measure the error between the ground-truth and estimated poses. To evaluate the performance over a whole dataset we build a pose estimation accuracy curve by thresholding errors over a range of thresholds. Then we integrate the area under the curve to get mean Average Accuracy (mAA) [42, 7]. We report mAA up to a 10-degree threshold for both rotation and translation as well as provide accuracy curve plots. Errors for rotation and translation are calculated in degrees [42, 40, 7].

#### 4.2.1 Evaluation on IMC-PT dataset

IMC-PT dataset [7] is a collection of photo-tourism images supplied with depth maps and poses reconstructed via SfM and MVS that features landmarks (mostly buildings). We use a full test set release that consists of 800 unique images from 8 different locations. By considering image pairs with co-visibility larger than 0.1 [7] we get 37k test image pairs.

Like on HPatches, DISK [15] descriptor shows the state-of-the-art performance on this dataset - hence we choose it.

We utilize a robust fundamental matrix estimator with DEGENSAC [43]. We calculate the essential matrix from the estimated fundamental matrix using ground-truth intrinsics and then recover the poses using OpenCV [41]. The tuning of hyper-parameters is performed on the validation subset of IMC-PT [7], see details in the supplementary material.

**Results.** Fig. 4a illustrates that our method consistently outperforms all methods other than DISK [15]. Comparison in Table 3 shows that we outperform self-supervised approaches like SuperPoint [19], Key.Net [20] and REKD [21] by a huge margin. We explain the gap between DISK [15] and our method by the difference in the strategies that methods employ to detect points. DISK [15] tends to densely detect points on semantically meaningful objects (mostly, buildings) whereas our method doesn't employ any knowledge of the scene and instead relies on the local properties of points resulting in sparsified detections. Given that IMC-PT [7] contains a lot of extreme viewpoint and scale changes the former strategy looks prevailing in this situation.

Methods	Rotation mAA (10°)	Translation mAA (10°)
Shi [24, 18] + DISK [15]	0.858	0.31
SIFT [30] + DISK [15]	0.83	0.299
SuperPoint [19] + DISK [15]	<b>0.873</b>	<b>0.318</b>
R2D2 [13] + DISK [15]	0.871	0.312
Key.Net [20] + DISK [15]	0.84	0.278
DISK [15]	<b>0.877</b>	<b>0.326</b>
REKD [21] + DISK [15]	0.848	0.274
Shi-NeSS + DISK [15]	<b>0.878</b>	<b>0.335</b>

Table 4: Evaluation on MegaDepth [16] with 2048 keypoints and full resolution images. We report mAA [42, 7] up to a 10 degrees threshold for rotation and translation. Best results are marked in **red**, 2nd best - in **green**, 3rd best - in **blue**.

#### 4.2.2 Evaluation on MegaDepth dataset

MegaDepth [16] dataset is another collection of photo-tourism images that also provides depth maps and poses. As IMC-PT dataset has a limited diversity of the scenes and their semantics and has only 800 unique images we create a custom test set from MegaDepth dataset to perform the assessment with a larger diversity of data. In particular, our test set consists of 7.5k image pairs with 6k unique images sampled from 25 scenes belonging to 5 semantically different categories. This test set doesn't have any intersections neither with validation nor with test sequences of IMC-PT.

Since both IMC-PT and MegaDepth belong to the category of outdoors/photo-tourism datasets their evaluation pipelines and hyper-parameters are shared.

**Results.** Contents of Fig. 4b and Table 4 show that evaluation on a more diverse set of data closes the gap between methods - now our method is marginally better than DISK [15]. Given that our method and DISK [15] share the same training set of MegaDepth [16] it is reasonable that they come on top in this evaluation. SuperPoint [19] is the second-best method in the category of methods that don't employ reconstructed correspondence labels. Although our gains in rotation estimation compared to it are marginal we obtain noticeably better translation estimates overall.

#### 4.2.3 Evaluation on ScanNet dataset

To assess the generalization ability of our method we perform the evaluation on ScanNet [17] dataset that contains indoor sequences with camera poses and depth maps. Following [12, 40] we create validation and test sets by sampling pairs from video sequences with different gaps between frames. Our test set consists of 21k image pairs with 39k unique images sampled from 100 test sequences of the dataset.

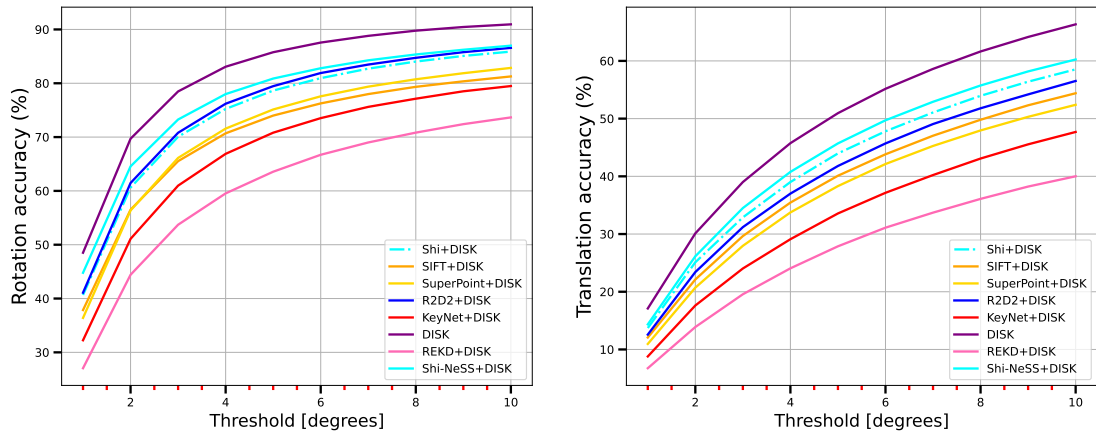
We perform the evaluation using HardNet [5] descriptor - on this dataset it shows performance that is superior to DISK [15] for every method.

As the ScanNet dataset is captured on a single RGB camera we employ a robust essential matrix estimator from OpenGV [44] - the rest of the pipeline remains the same as in previous evaluations. We use the validation subset of ScanNet for tuning hyper-parameters, see details in the supplementary material.

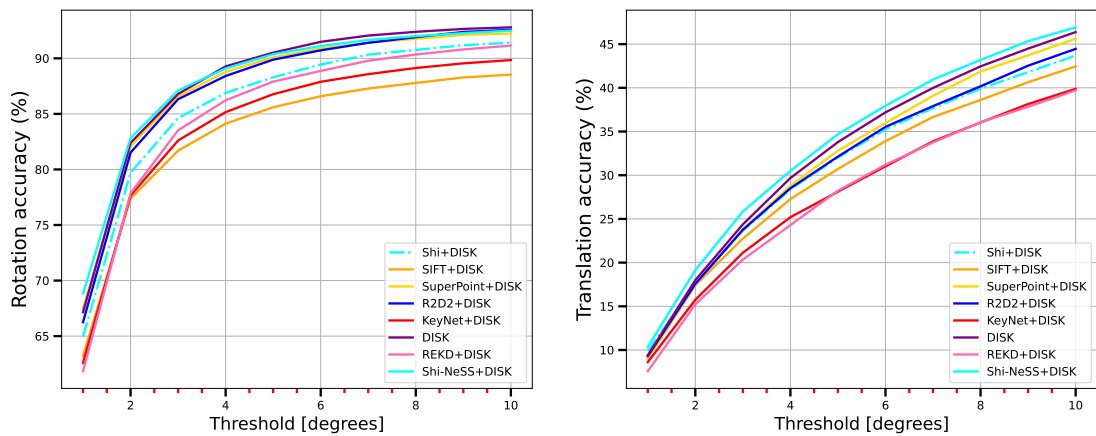
**Results.** Contrary to photo-tourism datasets that depict objects with a lot of texture, ScanNet [17] indoor environments contain a lot of surfaces with little to no texture. We believe that this is the main reason why DISK [15] shows significantly inferior performance on this set of data (see Table 5 and Fig. 4c). Our method, on the other hand, can consistently cope with the challenge and shows the second-best result. Given the large size of this test set it achieves considerable improvements compared to SuperPoint [19], Key.Net [20] and REKD [21] over all thresholds (see Fig. 4c). R2D2 [13] achieves the best performance on this dataset - we found that the method is able to provide consistent matches on images with little texture and poor illumination conditions by performing detection along the contours of objects.

Summarizing, the experiments show that Shi-NeSS is the only method among the top-three across all the datasets. It has better generalization ability compared to the state-of-the-art. Moreover, Shi-NeSS has the best performance among the self-supervised methods listed in Tab. 1.

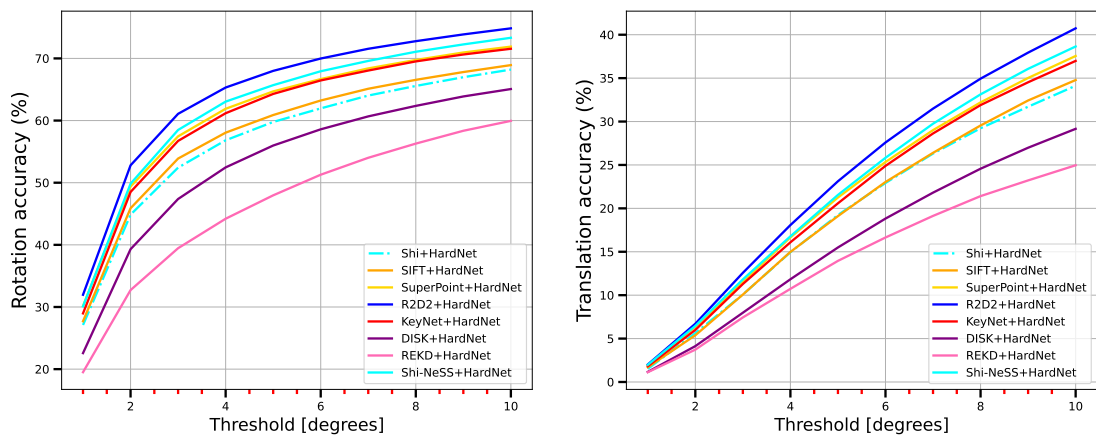




(a) Evaluation on IMC-PT [7].



(b) Evaluation on MegaDepth [16].



(c) Evaluation on ScanNet [17].

Figure 4: Evaluations with 2048 keypoints and full resolution images. We report relative pose estimation accuracy [42, 40, 7] in % for rotation (left) and translation (right).

Methods	Rotation mAA (10°)	Translation mAA (10°)
Shi [24, 18] + HardNet [5]	0.568	0.196
SIFT [30] + HardNet [5]	0.578	0.197
SuperPoint [19] + HardNet [5]	<b>0.611</b>	<b>0.217</b>
R2D2 [13] + HardNet [5]	<b>0.642</b>	<b>0.235</b>
Key.Net [20] + HardNet [5]	0.606	0.213
DISK [15] + HardNet [5]	0.528	0.162
REKD [21] + HardNet [5]	0.464	0.142
Shi-NeSS + HardNet [5]	<b>0.621</b>	<b>0.222</b>

Table 5: Evaluation on ScanNet [17] with 2048 keypoints and full resolution images. We report mAA [42, 7] up to a 10 degrees threshold for rotation and translation. Best results are marked in **red**, 2nd best - in **green**, 3rd best - in **blue**.

## 5 Conclusion

In this work, we proposed the Shi-NeSS detector that combines the hand-crafted Shi detector and the Neural Stability Score. The method doesn’t require any reconstructed correspondence labels and can be trained from arbitrary sets of images without the need for dataset pre-labeling. It achieves state-of-the-art performance on a variety of datasets and downstream tasks, has good generalization, and consistently outperforms other self-supervised methods. In the future, we plan to address the main limitation of our method - the lack of illumination invariance as well as use inferences from the evaluation of methods like DISK and R2D2 to improve our keypoint detection strategy. NeSS may be used as a weight in non-linear pose refinement or metric learning of feature descriptors.

## References

- [1] Raul Mur-Artal, Jose Maria Martinez Montiel, and Juan D Tardos. ORB-SLAM: a versatile and accurate monocular SLAM system. *IEEE Trans. Robotics*, 31(5):1147–1163, 2015.
- [2] Johannes L Schonberger and Jan-Michael Frahm. Structure-from-motion revisited. In *IEEE Conf. on Computer Vision and Pattern Recognition (CVPR)*, pages 4104–4113, 2016.
- [3] Robert Castle, Georg Klein, and David W Murray. Video-rate localization in multiple maps for wearable augmented reality. In *12th IEEE International Symposium on Wearable Computers*, pages 15–22, 2008.
- [4] Sven Middelberg, Torsten Sattler, Ole Untzelmann, and Leif Kobbelt. Scalable 6-dof localization on mobile devices. In *Eur. Conf. on Computer Vision (ECCV)*, pages 268–283, 2014.
- [5] Anastasiia Mishchuk, Dmytro Mishkin, Filip Radenovic, and Jiri Matas. Working hard to know your neighbor’s margins: Local descriptor learning loss. *Advances in Neural Information Processing Systems (NIPS)*, 30, 2017.
- [6] Yurun Tian, Xin Yu, Bin Fan, Fuchao Wu, Huub Heijnen, and Vassileios Balntas. Sosnet: Second order similarity regularization for local descriptor learning. In *IEEE Conf. on Computer Vision and Pattern Recognition (CVPR)*, pages 11016–11025, 2019.
- [7] Yuhe Jin, Dmytro Mishkin, Anastasiia Mishchuk, Jiri Matas, Pascal Fua, Kwang Moo Yi, and Eduard Trulls. Image matching across wide baselines: From paper to practice. *Intl. J. of Computer Vision*, 129(2):517–547, 2021.
- [8] Andrew P. Witkin. Scale-space filtering. In *IJCAI*, 1983.
- [9] Angela Dai, Matthias Nießner, Michael Zollhöfer, Shahram Izadi, and Christian Theobalt. Bundlerefusion: Real-time globally consistent 3d reconstruction using on-the-fly surface reintegration. *ACM Trans. Graph.*, 36(4):1, 2017.
- [10] Johannes L Schönberger, Enliang Zheng, Jan-Michael Frahm, and Marc Pollefeys. Pixelwise view selection for unstructured multi-view stereo. In *Eur. Conf. on Computer Vision (ECCV)*, pages 501–518. Springer International Publishing, 2016.
- [11] Kwang Moo Yi, Eduard Trulls, Vincent Lepetit, and Pascal Fua. Lift: Learned invariant feature transform. In *Eur. Conf. on Computer Vision (ECCV)*, pages 467–483. Springer, 2016.
- [12] Yuki Ono, Eduard Trulls, Pascal Fua, and Kwang Moo Yi. LF-Net: Learning local features from images. *Advances in Neural Information Processing Systems (NIPS)*, 31, 2018.

- [13] Jerome Revaud, Cesar De Souza, Martin Humenberger, and Philippe Weinzaepfel. R2d2: Reliable and repeatable detector and descriptor. In H. Wallach, H. Larochelle, A. Beygelzimer, F. d'Alché-Buc, E. Fox, and R. Garnett, editors, *Advances in Neural Information Processing Systems (NIPS)*, volume 32. Curran Associates, Inc., 2019.
- [14] Mihai Dusmanu, Ignacio Rocco, Tomas Pajdla, Marc Pollefeys, Josef Sivic, Akihiko Torii, and Torsten Sattler. D2-net: A trainable cnn for joint detection and description of local features. *arXiv preprint arXiv:1905.03561*, 2019.
- [15] Michał Tyszkiewicz, Pascal Fua, and Eduard Trulls. Disk: Learning local features with policy gradient. *Advances in Neural Information Processing Systems (NIPS)*, 33:14254–14265, 2020.
- [16] Zhengqi Li and Noah Snavely. Megadepth: Learning single-view depth prediction from internet photos. In *IEEE Conf. on Computer Vision and Pattern Recognition (CVPR)*, pages 2041–2050, 2018.
- [17] Angela Dai, Angel X Chang, Manolis Savva, Maciej Halber, Thomas Funkhouser, and Matthias Nießner. Scannet: Richly-annotated 3d reconstructions of indoor scenes. In *IEEE Conf. on Computer Vision and Pattern Recognition (CVPR)*, pages 5828–5839, 2017.
- [18] Jianbo Shi and Tomasi. Good features to track. In *IEEE Conf. on Computer Vision and Pattern Recognition (CVPR)*, pages 593–600, 1994.
- [19] Daniel DeTone, Tomasz Malisiewicz, and Andrew Rabinovich. SuperPoint: Self-supervised interest point detection and description. In *IEEE Conf. on Computer Vision and Pattern Recognition Workshops (CVPRW)*, pages 224–236, 2018.
- [20] Axel Barroso-Laguna, Edgar Riba, Daniel Ponsa, and Krystian Mikolajczyk. Key. net: Keypoint detection by handcrafted and learned cnn filters. In *IEEE Conf. on Computer Vision and Pattern Recognition (CVPR)*, pages 5836–5844, 2019.
- [21] Jongmin Lee, Byungjin Kim, and Minsu Cho. Self-supervised equivariant learning for oriented keypoint detection. In *IEEE Conf. on Computer Vision and Pattern Recognition (CVPR)*, pages 4847–4857, 2022.
- [22] Vassileios Balntas, Karel Lenc, Andrea Vedaldi, and Krystian Mikolajczyk. Hpatches: A benchmark and evaluation of handcrafted and learned local descriptors. In *IEEE Conf. on Computer Vision and Pattern Recognition (CVPR)*, pages 5173–5182, 2017.
- [23] Hans P. Moravec. Rover visual obstacle avoidance. In *Proceedings of the 7th International Joint Conference on Artificial Intelligence - Volume 2, IJCAI'81*, page 785–790, San Francisco, CA, USA, 1981. Morgan Kaufmann Publishers Inc.
- [24] C. Harris and M. Stephens. A combined corner and edge detector. In *Proceedings of the 4th Alvey Vision Conference*, pages 147–151, 1988.
- [25] Dorothea Blostein and Narendra Ahuja. A multiscale region detector. *Computer Vision, Graphics, and Image Processing*, 45(1):22–41, 1989.
- [26] Tony Lindeberg. Feature detection with automatic scale selection. *Intl. J. of Computer Vision*, 30(2):79–116, 1998.
- [27] Y. Dufournaud, C. Schmid, and R. Horaud. Matching images with different resolutions. In *IEEE Conf. on Computer Vision and Pattern Recognition (CVPR)*, volume 1, pages 612–618 vol.1, 2000.
- [28] Krystian Mikolajczyk and Cordelia Schmid. Indexing based on scale invariant interest points. In *Intl. Conf. on Computer Vision (ICCV)*, volume 1, pages 525–531. IEEE, 2001.
- [29] Krystian Mikolajczyk and Cordelia Schmid. An affine invariant interest point detector. In *Eur. Conf. on Computer Vision (ECCV)*, pages 128–142. Springer, 2002.
- [30] David G Lowe. Distinctive image features from scale-invariant keypoints. *Intl. J. of Computer Vision*, 60(2):91–110, 2004.
- [31] Herbert Bay, Tinne Tuytelaars, and Luc Van Gool. Surf: Speeded up robust features. In *Eur. Conf. on Computer Vision (ECCV)*, pages 404–417. Springer, 2006.
- [32] Pablo Fernández Alcantarilla, Adrien Bartoli, and Andrew J Davison. Kaze features. In *Eur. Conf. on Computer Vision (ECCV)*, pages 214–227. Springer, 2012.
- [33] Shishun Zhang, Longyu Zheng, and Wenbing Tao. Survey and evaluation of rgb-d slam. *IEEE Access*, 9:21367–21387, 2021.
- [34] Olaf Ronneberger, Philipp Fischer, and Thomas Brox. U-net: Convolutional networks for biomedical image segmentation. In *Medical Image Computing and Computer Assisted Intervention (MICCAI)*, pages 234–241. Springer, 2015.

- [35] Diederik P Kingma and Jimmy Ba. Adam: A method for stochastic optimization. In *ICLR (Poster)*, 2015.
- [36] Krystian Mikolajczyk, Tinne Tuytelaars, Cordelia Schmid, Andrew Zisserman, Jiri Matas, Frederik Schaffalitzky, Timor Kadir, and L Van Gool. A comparison of affine region detectors. *Intl. J. of Computer Vision*, 65:43–72, 2005.
- [37] Yannick Verdie, Kwang Yi, Pascal Fua, and Vincent Lepetit. Tilde: A temporally invariant learned detector. In *IEEE Conf. on Computer Vision and Pattern Recognition (CVPR)*, pages 5279–5288, 2015.
- [38] Xu Zhang, Felix X Yu, Svebor Karaman, and Shih-Fu Chang. Learning discriminative and transformation covariant local feature detectors. In *IEEE Conf. on Computer Vision and Pattern Recognition (CVPR)*, pages 6818–6826, 2017.
- [39] Krystian Mikolajczyk and Cordelia Schmid. A performance evaluation of local descriptors. *IEEE Trans. Pattern Anal. Machine Intell.*, 27(10):1615–1630, 2005.
- [40] Qianqian Wang, Xiaowei Zhou, Bharath Hariharan, and Noah Snavely. Learning feature descriptors using camera pose supervision. In *Eur. Conf. on Computer Vision (ECCV)*, pages 757–774. Springer International Publishing, 2020.
- [41] Gary Bradski. The opencv library. *Dr. Dobb’s Journal: Software Tools for the Professional Programmer*, 25(11):120–123, 2000.
- [42] Kwang Moo Yi, Eduard Trulls, Yuki Ono, Vincent Lepetit, Mathieu Salzmann, and Pascal Fua. Learning to find good correspondences. In *IEEE Conf. on Computer Vision and Pattern Recognition (CVPR)*, pages 2666–2674, 2018.
- [43] Ondrej Chum, Tomas Werner, and Jiri Matas. Two-view geometry estimation unaffected by a dominant plane. In *IEEE Conf. on Computer Vision and Pattern Recognition (CVPR)*, volume 1, pages 772–779. IEEE, 2005.
- [44] Laurent Kneip and Paul Furgale. Opengv: A unified and generalized approach to real-time calibrated geometric vision. In *IEEE Intl. Conf. on Robotics and Automation (ICRA)*, pages 1–8. IEEE, 2014.